Hindawi
Mathematical Problems in Engineering
Volume 2022, Article ID 2148947, 11 pages
https://doi.org/10.1155/2022/2148947

Research Article

Analytical Solution for Elastic Analysis around an Ellipse with Displacement-Controlled Boundary

Jingjing Yin,[1] Huaijian Li,[2] Lingdi Kong,[2] Junwei Cheng,[2] Tonghui Niu,[3] Xiaonan Wang,[2] and Peizhi Zhuang[4]

[1]*School of Transportation, Shandong Jianzhu University, Jinan 250101, China*
[2]*Shandong Hi-Speed Group Co. Ltd, Jinan 250014, China*
[3]*Shandong Hi-Speed Transportation Construction Group Co.Ltd, Jinan 250101, China*
[4]*School of Qilu Transportation, Shandong University, Jinan 250110, China*

Correspondence should be addressed to Peizhi Zhuang; zhuangpeizhi@sdu.edu.cn

Received 26 October 2021; Revised 28 April 2022; Accepted 9 May 2022; Published 8 June 2022

Academic Editor: Federico Guarracino

This paper presents novel analytical solutions for the analysis of an elliptical cavity within an infinite plane under plane strain conditions, considering typical displacement-controlled boundaries at the inner cavity and biaxial stresses at infinity. The problem is investigated by the plane theory of elasticity using Muskhelishvili's complex variable method. The complex displacement boundary conditions are represented using the conformal mapping technique and Fourier series, and stress functions are evaluated using Cauchy's integral formula. The proposed solutions are validated at first by comparing them with other existing solutions and then used to show the influences of displacement vectors on the distributions of induced stresses and displacements. The new solutions may provide useful analytical tools for stress and displacement analysis of an elliptical hole/opening in linear elastic materials which are common in many engineering problems.

1. Introduction

The stress and deformation analysis around a cavity is a typical boundary-value problem, and it is of great interest in the design and analysis of many engineering problems [1–3]. In general, the stress and deformation fields around a cavity can be obtained by means of solving a governing equation system that is constituted of stress equilibrium equations, displacement compatibility conditions, and stress-strain relationships with response to given boundary conditions. The usual boundary conditions can be broadly categorised into three groups, including stress-boundary, displacement-boundary, and mixed-boundary conditions [3–7]. This paper aims to provide novel analytical solutions for the elastic analysis of an ellipse deforming with specified displacements in an infinite plane under biaxial far-field stresses.

It is instructive to review the developments of relevant solutions for the analysis of an elliptical cavity before the derivation. Elastic solutions for an infinite plate with an elliptical cavity were first given by Kolosoff [7] and Inglis [8] around a century ago. The solution of Inglis [8] provided a theoretical basis for the development of the well-known Griffith's energy criterion [9] in fracture mechanics. Later, Stevenson [10] independently carried out some two-dimensional analyses on similar problems in curvilinear coordinate systems. The elliptic coordinate system and the complex variable theory were used in these solutions, and judicious selection of the complex potentials is necessarily required and greatly determines the solution accuracy [7]. Alternatively, a more powerful and general method was developed by deducing the potentials directly from the boundary conditions as elaborated in the monograph of Muskhelishvili [3]. Based on the complex variable theory and some more advanced mathematic techniques, this branch of methods is capable of dealing with problems with complex stress boundary conditions and can also be extensively applied in the analysis of cavities with various shapes. Based on these methods, a number of analytical

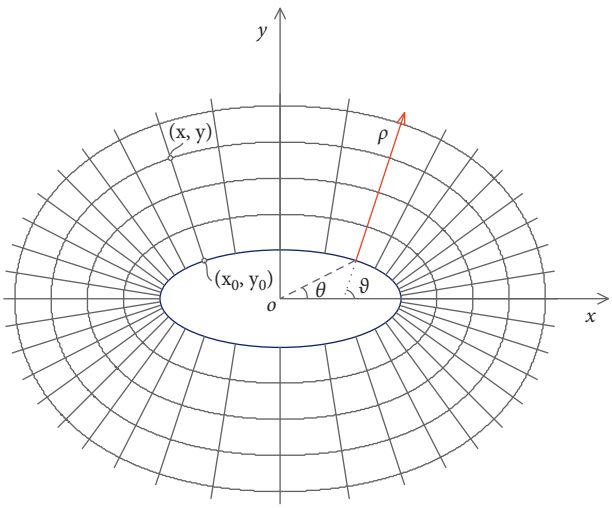

Figure 1: Geometry boundaries and coordinate systems.

solutions have been developed over the past few decades, for example, elastic solutions for two-dimensional analysis of cavities with various shapes under complex stress boundary conditions [2, 3] and elastic solutions for cavities in a semiinfinity plane [11–13]. These solutions provided important and solid theoretical foundations for many areas, for example, analyses of crack propagation and stress concentration [2, 14–17]. In the geotechnical engineering, elastic solutions for cavity loading/unloading analysis were often employed in the static stability analysis and calculation of static stress and deformation fields around wellbores [1, 18], tunnels [19, 20], piles [21–23], and many other underground structures/openings.

Previous solutions for the analysis around an ellipse mostly focused on the problem under the stress-controlled type of boundary conditions, for example, the analyses of an infinite elastic plate with a traction-free [8, 14, 24, 25] or uniformly loaded [2, 3, 26] elliptical hole subjected to biaxial far-field loading. In fact, in some engineering problems, the inner elliptical cavity may also likely deform with specified displacements [27, 28], for instance, the membrane expansion of a flat dilatometer and the radial expansion process of bio-inspired soil penetrometers/robots in the ground [29, 30]. Zhou et al. [17] presented an analytical solution for the elastic analysis of a flat elliptical cavity with small displacements in the direction parallel to one coordinate axis and applied the solution to the modelling of in-situ dilatometer tests. However, solutions for the analysis of an ellipse with more general types of displacement-controlled boundary conditions were rarely reported in the literature.

In this study, considering general types of displacement-controlled boundary conditions at the inner elliptical cavity and biaxial stresses at infinity, analytical solutions for the elastic stresses and displacements are derived for the first time. The problem is defined at first, which is followed by the solving process using the complex variable theory of elasticity and the conformal mapping technique. Then, the proposed solutions are validated with other existing solutions in the literature and discussed briefly. Finally, conclusions are drawn in the last section.

2. Problem Definition

An elliptical cavity within an infinite plane is considered (Figure 1). The inner cavity deforms with given displacements under plane strain conditions, and nonequal biaxial stresses are applied at infinity. It is assumed that the cavity is surrounded by isotropic, linear elastic materials. For convenience, both Cartesian coordinates (o, x, y) and orthogonal curvilinear coordinates (o, ρ, ϑ), which have the same origin in the centre of the ellipse (i.e., point o), are employed [31] as shown in Figure 1. ρ represents the distance from the inner boundary to a particular point along the direction normal to the innermost cavity wall. ϑ is the angle from the positive x-axis direction to the direction that is normal to the inner elliptical boundary ($\vartheta \in [0, 2\pi]$).

The paralleled elliptic coordinates in Figure 1 were proposed by Unger [32, 33], which consist of a series of naturally orthogonal oval shape lines, paralleling to the innermost ellipse, and radial lines, perpendicular to the innermost cavity. Points in the new coordinates system can be expressed as

$$\begin{aligned} x &= x_0 + \rho \cos \vartheta, \\ y &= y_0 + \rho \sin \vartheta, \end{aligned} \tag{1}$$

where (x_0, y_0) represents coordinates of points on the initial ellipse as defined in the following equation:

$$\frac{{x_0}^2}{a^2} + \frac{{y_0}^2}{b^2} = 1, \left(x_0 = a \cos t, y_0 = b \sin t\right), \text{and } a \neq 0, b \neq 0, \tag{2}$$

where "t" represents the eccentric angle of an ellipse (see Figure 2). "a" and "b" are the semimajor axis and the semiminor axis, respectively.

The two coordinate systems can be linked with $\tan \vartheta = a/b \tan t$ so that the inner ellipse can be described in the curvilinear coordinates as

$$\begin{aligned} x_0 &= \frac{a^2 \cos \vartheta}{\sqrt{H}}, \\ y_0 &= \frac{b^2 \sin \vartheta}{\sqrt{H}}, \quad \left(H = a^2 \cos^2 \vartheta + b^2 \sin^2 \vartheta\right). \end{aligned} \tag{3}$$

To complete the transformation between these two coordinate systems, the concept of metric coefficients [5, 6] is applied. The strain tensor, strain-displacement relations, and equilibrium equations in the paralleled elliptic coordinate system can be readily established with the general relations for orthogonal curvilinear coordinate systems [6] as

$$\begin{aligned} \varepsilon_{\rho\rho} &= \frac{\partial u_\rho}{\partial \rho}, \\ \varepsilon_{\vartheta\vartheta} &= \frac{1}{\rho + F(\vartheta)} \left[\frac{\partial u_\vartheta}{\partial \vartheta} + u_\rho\right], \\ \varepsilon_{\rho\vartheta} &= \frac{1}{2} \left[\frac{1}{\rho + F(\vartheta)} \frac{\partial u_\rho}{\partial \vartheta} + \frac{\partial u_\vartheta}{\partial \rho} - \frac{u_\vartheta}{\rho + F(\vartheta)}\right], \end{aligned} \tag{4}$$

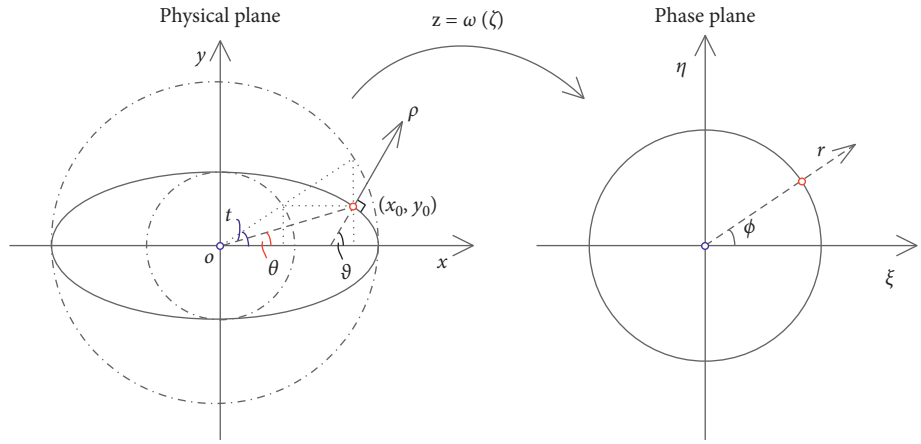

Figure 2: Mapping function for an ellipse.

where $F(\vartheta) = a^2b^2/H^{3/2}$. u_ρ and u_ϑ are displacement components in the normal and the tangential directions of the parallel-elliptic coordinates, respectively. $\varepsilon_{\rho\rho}$, $\varepsilon_{\vartheta\vartheta}$, and $\varepsilon_{\rho\vartheta}$ are strain components in the normal, tangential, and axial directions of the parallel-elliptic coordinates, respectively. In fact, $F(\vartheta)$ represents the radius of curvature of the corresponding point at the cavity wall.

The stress equilibrium equations along the normal and the tangential directions with the absence of body force for the plane strain problem can be expressed as

$$\begin{aligned} &\frac{\partial \sigma_{\rho\rho}}{\partial \rho} + \frac{1}{\rho + F(\vartheta)} \frac{\partial \sigma_{\rho\vartheta}}{\partial \rho} + \frac{\sigma_{\rho\rho} - \sigma_{\vartheta\vartheta}}{\rho + F(\vartheta)} = 0, \\ &\frac{1}{\rho + F(\vartheta)} \frac{\partial \sigma_{\vartheta\vartheta}}{\partial \vartheta} + \frac{\partial \sigma_{\rho\vartheta}}{\partial \rho} + \frac{2\sigma_{\rho\vartheta}}{\rho + F(\vartheta)} = 0, \end{aligned} \tag{5}$$

where $\sigma_{\rho\rho}$, $\sigma_{\vartheta\vartheta}$, and $\sigma_{\rho\vartheta}$ are stress components in the normal, tangential, and axial directions within the parallel-elliptic coordinates, respectively.

3. Elastic Stress and Displacement Solutions

3.1. Complex Variable Theory for Elasticity. The complex variable theory provides a powerful theoretical tool for dealing with a broad class of two-dimensional boundary-value problems in elasticity [34]. From its first systematic use in elasticity by Kolossof as early as 1909, this method experienced great developments and improvements in both theory and application [2, 3, 35]. Briefly, it has been found in the plane theory of elasticity that stresses and displacements can be expressed by means of one single auxiliary function $U(x, y)$ (e.g., Airy function), and every biharmonic function $U(x, y)$ may be represented in a simple manner with the help of two analytic functions of a complex variable $z = x + iy$ ($\overline{z} = x - iy$, $i = \sqrt{-1}$) such as $\varphi(z)$ and $\chi(z)$ [3], and it can be expressed as

$$U(x, y) = \mathrm{Re}[\overline{z}\varphi(z) + \chi(z)], \tag{6}$$

where Re[...] represents the symbol to take the real part of a complex number.

Then, the stresses and displacements (free of body forces) can be represented by the first-order and the second-order derivatives of $\varphi(z)$ and $\chi(z)$ as

$$\sigma_x^e + \sigma_y^e = 4\mathrm{Re}[\Phi(z)], \tag{7}$$

$$\sigma_y^e - \sigma_x^e + 2i\tau_{xy}^e = 2[\overline{z}\Phi\prime(z) + \Psi(z)], \tag{8}$$

$$2G\left(u_x^e + iu_y^e\right) = [\kappa\varphi(z) - z\overline{\varphi\prime(z)} - \overline{\psi(z)}], \tag{9}$$

where σ_x^e, σ_y^e, and τ_{xy}^e are elastic stress components, and u_x^e and u_y^e are elastic displacement components. $\Phi(z)$ and $\Psi(z)$ are usually referred to as the Kolosov–Muskhelishvili complex potentials. $\Phi(z) = \varphi'(z)$, $\Psi(z) = \psi'(z)$, and $\psi(z) = \chi'(z)$. $\kappa = 3 - 4\nu$ for plane strain problem. G is the elastic shear modulus, and ν is Poisson's ratio.

The conformal mapping technique is able to convert the region with a contour in various shapes in the physical plane to the region bounded by the unit circle with origin in the centre of the phase plane [34]. For the problem of an infinite region with a simple contour inside, it is convenient to map the exterior of the cavity in the physical plane onto the exterior region of the unit circle in the phase plane. As illustrated in Figure 2, the conformal mapping function of (10) can conformally map the exterior of an elliptical cavity in the physical plane onto the exterior region of the unit circle "γ" in the phase plane.

$$z = x + iy = \omega(\zeta) = R\left(\zeta + \frac{m}{\zeta}\right), \tag{10}$$

where $\zeta = \xi + i\eta = re^{i\phi}$ describing the position vectors in the phase plane (o, r, ϕ) as illustrated in Figure 2. ξ and η are the real part and the imaginary part of the complex number ζ, respectively. r and ϕ are the modulus and the argument of ζ, respectively. $R = a + b/2$, $m = a - b/a + b$. By relating to the previously defined curvilinear coordinates, the corresponding positions of points in the phase plane and the physical plane can be linked with (11) and (12).

$$x = x_0 + \rho\cos\vartheta = R\left(r + \frac{m}{r}\right)\cos\phi, \tag{11}$$

$$y = y_0 + \rho\sin\vartheta = R\left(r - \frac{m}{r}\right)\sin\phi. \tag{12}$$

Based on the determinacy analysis of these complex potentials within a given stress state and/or an admissible displacement field, the general forms of the Kolosov–Muskhelishvili for multiple-connected regions and single-connected regions were given by Muskhelishvili [3]. For addressing the problem concerned in this paper, the general solutions for an infinite plane with a single hole are as follows:

$$\varphi(\zeta) = \Gamma R\zeta - \frac{X + iY}{2\pi(1+\kappa)}\ln\zeta + \varphi_0(\zeta), \tag{13}$$

$$\psi(\zeta) = \Gamma' R\zeta + \frac{\kappa(X - iY)}{2\pi(1+\kappa)}\ln\zeta + \psi_0(\zeta), \tag{14}$$

$$\begin{aligned}\Gamma' &= \frac{-(N_1 - N_2)e^{-2i\Lambda}}{2},\\ \Gamma &= \frac{(N_1 + N_2)}{4},\end{aligned} \tag{15}$$

where N_1 and N_2 represent the principal stresses at infinity (tension for positive). Λ is the angle between N_1 and the x-axis direction, taking the x-axis direction to the direction of N_1 of anticlockwise rotation as positive. $\varphi_0(\zeta)$ and $\psi_0(\zeta)$ are holomorphic in the whole concerned region. X and Y represent components of the resultant stress vector in x-axis and y-axis directions, respectively. Accordingly, the complex potentials are related to the stress boundary conditions. For more details about the derivation of equations (13)–(15), refer to Chapter 14 of the reference [3].

By expressing the formulas from equations (7) to (9) in terms of ζ, the stress and displacement components can be expressed with

$$\begin{aligned}\sigma_x^e + \sigma_y^e &= 4\mathrm{Re}[\Phi(\zeta)],\\ \sigma_y^e - \sigma_x^e + 2i\tau_{xy}^e &= 2\left[\frac{\overline{\omega(\zeta)}}{\omega\prime(\zeta)}\Phi\prime(\zeta) + \Psi(\zeta)\right],\\ 2G\left(u_x^e + iu_y^e\right) &= \left[\kappa\varphi(\zeta) - \frac{\omega(\zeta)}{\overline{\omega\prime(\zeta)}}\overline{\varphi\prime(\zeta)} - \overline{\psi(\zeta)}\right],\end{aligned} \tag{16}$$

where $\Phi(\zeta) = \varphi'(\zeta)/\omega'(\zeta)$, $\Psi(\zeta) = \psi'(\zeta)/\omega'(\zeta)$.

Points between the physical plane and the phase plane can be correspondingly related by (11) and (12). In addition, based on the mapping function, required functions in the above representations are obtained as

$$\overline{\omega(\zeta)} = \overline{\omega}(\overline{\zeta}) = R\left(\overline{\zeta} + \frac{m}{\zeta}\right) = R\left(\frac{r^2}{\zeta} + \frac{m\zeta}{r^2}\right),$$

$$\omega\prime(\xi) = R\left(1 - \frac{m}{\zeta^2}\right), \qquad \overline{\omega\prime(\zeta)} = R\left(1 - \frac{m\zeta^2}{r^4}\right), \tag{17}$$

where $\zeta\cdot\overline{\zeta} = r^2$ in the phase plane ($\overline{\zeta}$ is the conjugate complex of ζ).

3.2. Complex Potentials for an Ellipse Deforming with Given Displacements

3.2.1. Inner Displacement Boundary Conditions. The displacement boundary condition consists of two basic parameters, including the magnitude and the direction of movement of each point. It is assumed that the initial position of points on the inner ellipse (x_0, y_0) is defined by the following equation:

$$\frac{{x_0}^2}{{a_0}^2} + \frac{{y_0}^2}{{b_0}^2} = 1, \tag{18}$$

where a_0 and b_0 denote the semimajor axis and the semiminor axis of the initial elliptical cavity, respectively.

It is assumed that the cavity after deformation is still in an elliptical shape, and its axes' directions coincide with the initial ellipse. (19) describes the geometry of the deformed cavity.

$$\frac{{x_1}^2}{{a_1}^2} + \frac{{y_1}^2}{{b_1}^2} = 1. \tag{19}$$

Note that, in theory, the deformed cavity can also be defined in other shapes by replacing (19) with specified equations. Based upon (18) and (19), two typical displacement-controlled boundary conditions are considered as follows.

Case 1. Inner boundary displacements being normal to the initial surface

In this case, it is assumed that points on the inner ellipse move outwards along the direction perpendicular to the initial cavity wall, and the magnitude of the boundary displacements is determined by the given initial and final position of the cavity (Figure 3). In addition, nonequal biaxial stresses are applied at infinity.

In this case, the displacement components can be expressed using the orthogonal parallel-elliptic coordinates as

$$u_x^e + iu_y^e = \rho(\vartheta)\cos\vartheta + i\rho(\vartheta)\sin\vartheta = \rho(\vartheta)e^{i\vartheta}. \tag{20}$$

Note that the normal distance ($\rho(\vartheta)$) from the initial cavity rims to the ellipse after deformation varies with angle because the circumference of the deformed ellipse does not parallel to the original ellipse. Solving (1) and (19) gives

$$\rho(\vartheta) = \frac{\left[-\left(x_0 b_1^2 cos\vartheta + y_0 a_1^2 \sin\vartheta\right) + \sqrt{\left(x_0 b_1^2 cos\vartheta + y_0 a_1^2 \sin\vartheta\right)^2 - \left(a_1^2 \sin^2\vartheta + b_1^2 \cos^2\vartheta\right)\left(x_0^2 b_1^2 + y_0^2 a_1^2 - a_1^2 b_1^2\right)}\right]}{\left(a_1^2 \sin^2\vartheta + b_1^2 \cos^2\vartheta\right)}. \quad (21)$$

As given in (9), the relation between the complex potentials and the displacement boundary is rewritten as

$$2Gg(x, y) = 2G\left(u_x^e + iu_y^e\right)|_\gamma = \kappa\varphi(\sigma) - \frac{\omega(\sigma)}{\omega'(\sigma)}\overline{\varphi'(\sigma)} - \overline{\psi(\sigma)}. \quad (22)$$

To transform the displacement boundary in Eq. (20) to the phase plane, the angle ϑ is related to the argument ϕ of the phase plane on the basis of (11) and (12) as

$$\tan\vartheta = \frac{a_0^2(1-m)}{b_0^2(1+m)} tan\phi. \quad (23)$$

All the trigonometric functions can be expressed with the above tangent function. As a result, (20) becomes a function of the variable of argument ϕ. The resultant displacement boundary function $g(\phi)$ is continuous in the range of $0 \le \phi \le 2\pi$ along the circumference of the unit circle γ in the phase plane and satisfies the Dirichlet conditions. Therefore, it is convenient to reexpress it based on the expansion of the Fourier series in terms of σ ($\sigma = e^{i\phi}$) [3, 17]. The series-type representation is

$$g(\phi) = g_1(\phi) + ig_2(\phi) = u_x^e + iu_y^e = \sum_{-\infty}^{+\infty} A_n e^{in\phi} = \sum_{-\infty}^{+\infty} A_n \sigma^n$$
$$= \sum_{n=1}^{+\infty} \frac{A_{-n}}{\sigma^n} + A_0 + \sum_{n=1}^{+\infty} A_n \sigma^n, \quad n = 1, 2, 3, \cdots, \quad (24)$$

where $A_n = 1/2\pi \int_0^{2\pi} [g_1(\phi) + ig_2(\phi)] e^{-in\phi} d\phi$ which are the coefficients of the Fourier series. $g_1(\phi)$ is an even function, and $g_2(\phi)$ is an odd function. As a result, A_n are real numbers based on the property of the Fourier series. Furthermore, based on the consistency requirement of (20) and (24) in parity with respect to the variable of σ, it can be concluded that the even terms of the Fourier series in (24) should equal to zero. Hence, $g(\phi)$ can be simplified to be

$$g(\phi) = \sum_{n=1}^{+\infty} \frac{A_{-(2n-1)}}{\sigma^{2n-1}} + \sum_{n=1}^{+\infty} A_{2n-1} \sigma^{2n-1}. \quad (25)$$

In the special case of Case 1, the cavity deforms with the same normal displacements.

In this special case, points on the initial cavity wall move outwards in the normal direction with the same distance. In another word, a constant value of ρ is assumed. Hence, the boundary condition becomes

$$u_x^e + iu_y^e = \rho \cos\vartheta + i\rho \sin\vartheta = \rho e^{i\vartheta}, \ (\rho = \text{const}). \quad (26)$$

The same procedure can be followed as above to transform this boundary condition into Fourier series, and the same form of representation as (25) can be obtained but with different coefficients.

Case 2. Displacements of the inner ellipse pointing outwards from the centre of the initial ellipse

In this case, material points on the initial ellipse move outwards along the radial direction of the cylindrical coordinate system (see Figure 4). Therefore, a combination use of the Cartesian coordinate system and the cylindrical coordinate system is adopted in this analysis. Similarly, the coordinate positions can be expressed in terms of the centre angle θ as

$$x = x_0 + l \cos\theta,$$
$$y = y_0 + l \sin\theta, \quad (27)$$

where $x_0 = ab \cos\theta/\sqrt{T}$, $y_0 = ab \sin\theta/\sqrt{T}$, and $T = b^2\cos^2\theta + a^2\sin^2\theta$. l represents the distance from one given point to the corresponding point on the inner ellipse along the radial axis direction.

Subsequently, the given boundary conditions can be expressed as

$$u_x^e + iu_y^e = l(\theta)\cos\theta + il(\theta)\sin\theta = l(\theta)e^{i\theta}. \quad (28)$$

And, similarly

$$l(\theta) = \frac{\left[\begin{array}{c} -\left(x_0 b_1^2 cos\theta + y_0 a_1^2 \sin\theta\right) \\ + \sqrt{\left(x_0 b_1^2 cos\theta + y_0 a_1^2 \sin\theta\right)^2 - \left(a_1^2 \sin^2\theta + b_1^2 \cos^2\theta\right)\left(x_0^2 b_1^2 + y_0^2 a_1^2 - a_1^2 b_1^2\right)} \end{array}\right]}{\left(a_1^2 \sin^2\theta + b_1^2 \cos^2\theta\right)}. \quad (29)$$

Then, the centre angle is related to the variable ϕ belonging to the phase plane with

$$\tan\theta = \frac{(1-m)}{(1+m)} tan\phi. \quad (30)$$

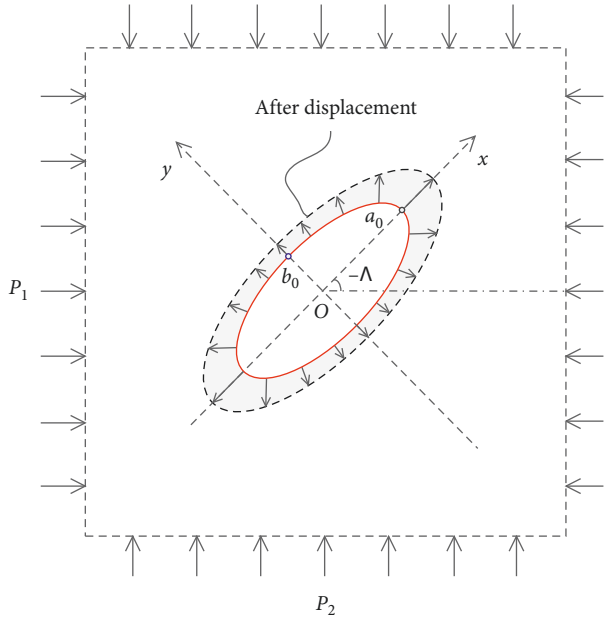

Figure 3: Schematic diagram of the boundary conditions (Case 1).

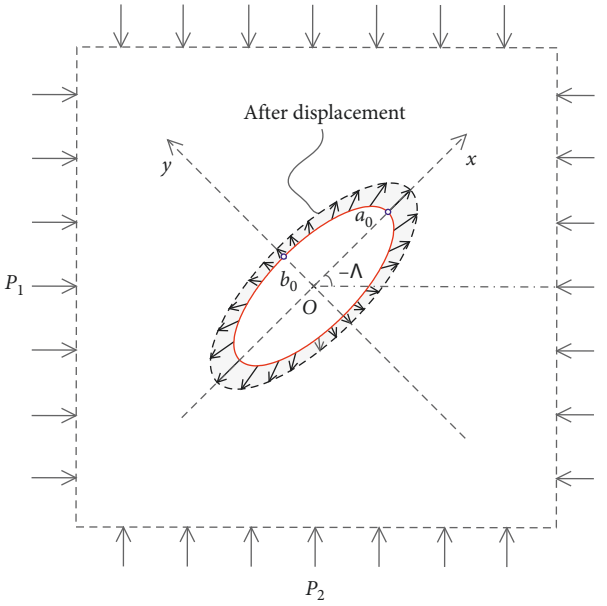

Figure 4: Schematic diagram of the boundary conditions (Case 2).

Then, following the same procedure, the displacement boundary conditions can be expressed in the same form as (25) with different coefficients.

3.2.2. Biaxial Far-Field Stress Boundary Conditions. Biaxial compression stresses (P_1 and P_2) are applied at infinity (far away from the cavity comparing with the cavity size), and the semimajor axis direction of the ellipse takes a clockwise angle Λ to the direction of the principal stress P_1. As a result,

$$\Gamma = \frac{-(P_1 + P_2)}{4}, \Gamma' = \frac{(P_1 - P_2)e^{-2i\Lambda}}{2}, \text{(at infinity)}. \tag{31}$$

3.2.3. Derivation of the Complex Potentials. To represent the given type of displacement boundary conditions in terms of the complex potentials, (9) is rewritten as

$$2Gg(x,y) = 2G(g_1 + ig_2) = \kappa\varphi(\zeta) - \frac{\omega(\zeta)}{\omega'(\zeta)}\overline{\varphi'(\zeta)} - \overline{\psi(\zeta)}. \tag{32}$$

With this representation and general forms of $\varphi(\zeta)$ and $\psi(\zeta)$ (i.e., Eq. (13) and Eq. (15)), Muskhelishvili [3] (see Chapter 15) gave the general representations for the complex

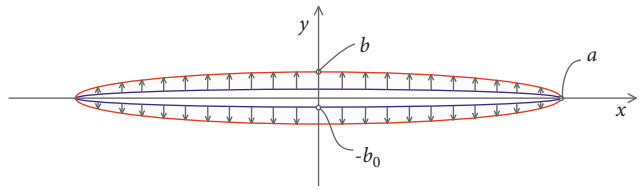

Figure 5: Normal directions of points on a flat cavity.

potentials with the displacement-type boundary conditions for the problem of an elliptical cavity in an infinite plane.

$$\varphi_0(\zeta) = -\frac{2G}{\kappa}\frac{1}{2\pi i}\int_\gamma \frac{g}{\sigma - \zeta}d\sigma + (m\Gamma + \overline{\Gamma}')\frac{R}{\kappa\zeta},$$

$$\psi_0(\zeta) = \frac{G}{\pi i}\int_\gamma \frac{\overline{g}}{\sigma - \zeta}d\sigma + \Gamma R\left(\frac{\kappa}{\zeta} - \zeta\frac{1+m^2}{\zeta^2 - m}\right) + \frac{X + iY}{2\pi(1+\kappa)}\frac{1+m^2}{(\zeta^2 - m)} - \zeta\frac{1+m\zeta^2}{\zeta^2 - m}\varphi_0'(\zeta) + \psi_0'(\infty),$$

$$\psi_0(\infty) = -\frac{G}{\pi i}\int_\gamma \frac{\overline{g}_0}{\sigma}d\sigma = -\frac{G}{\pi i}\int_\gamma \frac{\overline{g}}{\sigma}d\sigma + \frac{m(X+iY)}{2\pi(1+\kappa)}. \tag{33}$$

Based on these formulas and the given boundary conditions, complex potentials for the defined problem can be obtained using the Cauchy integral method as follows:

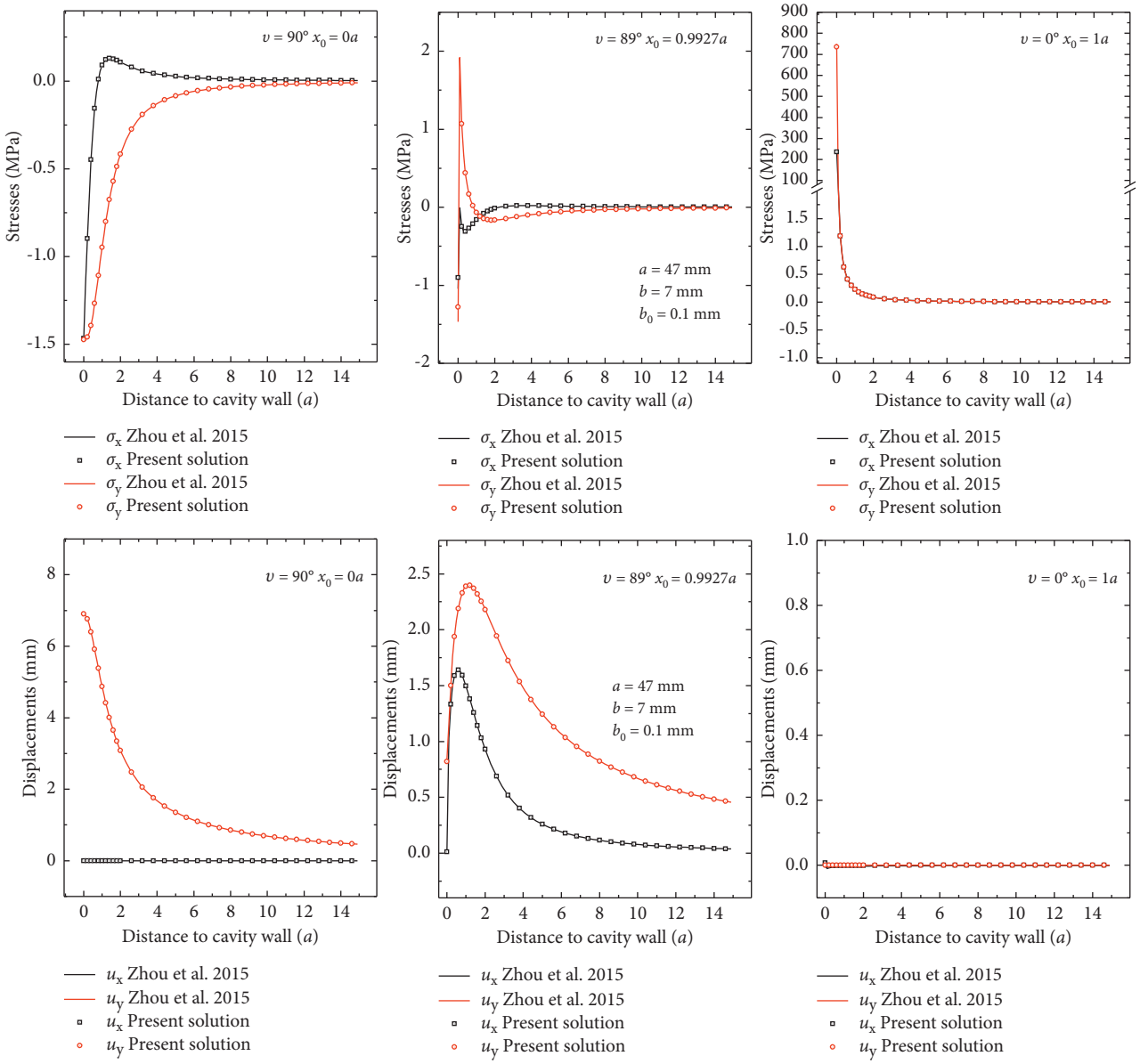

Figure 6: Validation of the solution with displacement boundary.

$$
\begin{aligned}
\varphi_0(\zeta) &= \frac{2G}{\kappa}\sum_{n=1}^{+\infty}\frac{A_{-(2n-1)}}{\zeta^{2n-1}} + \left[-m\frac{(P_1+P_2)}{4} + \frac{(P_1-P_2)e^{2i\Lambda}}{2}\right]\frac{R}{\kappa\zeta},\\
\psi_0(\zeta) &= -2G\sum_{n=1}^{+\infty}\frac{\overline{A}_{2n-1}}{\zeta^{2n-1}} + R\frac{(P_1+P_2)}{4}\left(\frac{\kappa}{\zeta} - \zeta\frac{1+m^2}{\zeta^2-m}\right)\\
&\quad - \zeta\frac{1+m\zeta^2}{\zeta^2-m}\left\{-\frac{2G}{\kappa}\sum_{n=1}^{+\infty}(2n-1)\frac{A_{-(2n-1)}}{\zeta^{2n}} + \left[m\frac{(P_1+P_2)}{4} - \frac{(P_1-P_2)e^{2i\Lambda}}{2}\right]\frac{R}{\kappa\zeta^2}\right\},\\
\varphi(\zeta) &= -\frac{(P_1+P_2)}{4}R\zeta + \frac{2G}{\kappa}\sum_{n=1}^{+\infty}\frac{A_{-(2n-1)}}{\zeta^{2n-1}} + \left[-m\frac{(P_1+P_2)}{4} + \frac{(P_1-P_2)e^{2i\Lambda}}{2}\right]\frac{R}{\kappa\zeta},\\
\psi(\zeta) &= \frac{(P_1-P_2)e^{-2i\Lambda}}{2}R\zeta - 2G\sum_{n=1}^{+\infty}\frac{\overline{A}_{2n-1}}{\zeta^{2n-1}} + R\frac{(P_1+P_2)}{4}\left(\frac{\kappa}{\zeta} - \zeta\frac{1+m^2}{\zeta^2-m}\right)\\
&\quad - \zeta\frac{1+m\zeta^2}{\zeta^2-m}\left\{-\frac{2G}{\kappa}\sum_{n=1}^{+\infty}(2n-1)\frac{A_{-(2n-1)}}{\zeta^{2n}} + \left[m\frac{(P_1+P_2)}{4} - \frac{(P_1-P_2)e^{2i\Lambda}}{2}\right]\frac{R}{\kappa\zeta^2}\right\}.
\end{aligned}
\tag{34}
$$

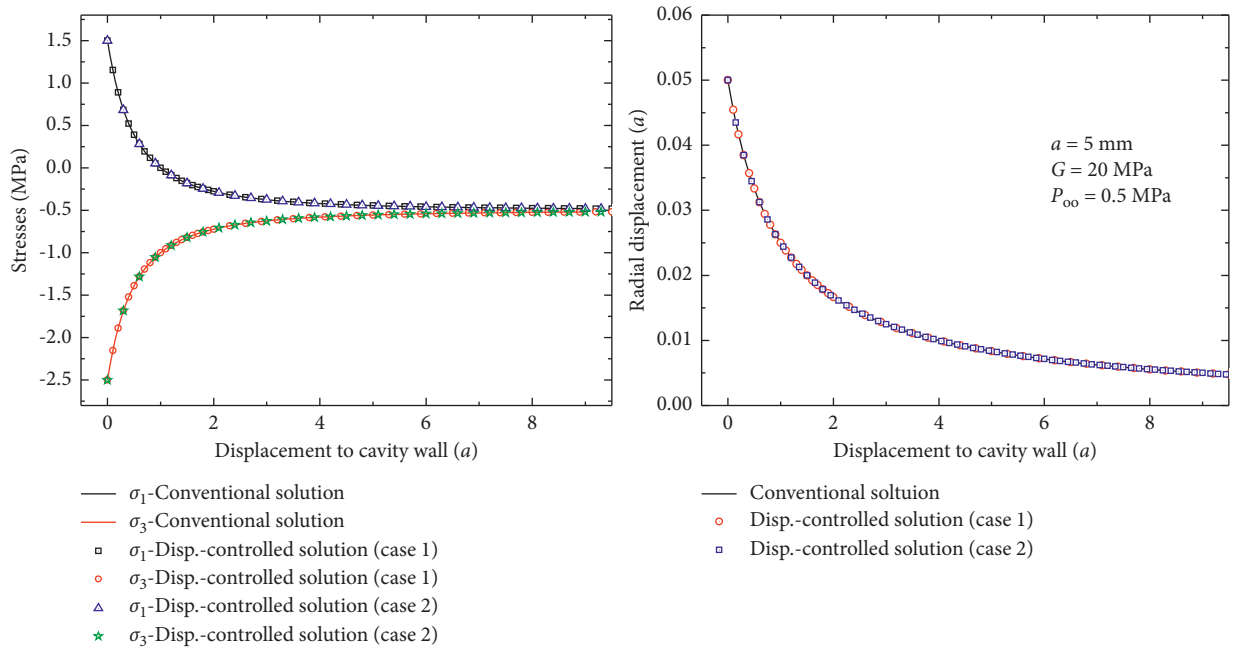

Figure 7: Comparison with the conventional solution for the circular cavity.

4. Results Analysis

In this section, the proposed solutions are validated by comparing them with existing solutions for special conditions at first. Then, some results are presented to show the differences between the concerned two types of displacement boundary conditions.

4.1. Comparison with the Solution for a Flat Cavity. The analytical solution for Case 1 (i.e., displacements normal to the initial cavity wall) is compared with the solution proposed by Zhou et al. [17]. Their solution was designed for a flat elliptical cavity undergoing small displacements in the direction parallel to one coordinate axis, and the given final shape of the inner cavity is still in an elliptical shape. The boundary condition is defined in Eq. (35). Note that the defined moving directions of the inner boundary in the solution of Zhou et al. [17] are not exactly the same as those defined in Case 1 of this paper. Nevertheless, it is anticipated that they could give approximately the same results when the ellipse is very flat. As illustrated in Figure 5, the normal directions of the inner flat ellipse are almost parallel to the axis direction in a large angular scope.

$$u_x^e + iu_y^e|_\gamma = \frac{-ia(b-b_0)sin\phi}{\sqrt{\beta^2 b_0{}^2 + (a^2 - \beta^2 b_0{}^2)sin^2\phi}}. \tag{35}$$

Taking the elastic modulus as 15 MPa and Poisson's ratio as 0.5, comparisons between these two solutions are carried out as shown in Figure 6. With the given geometry parameters, the normal direction of the inner flat ellipse just rotated 1° away from the direction of y-axis even when $x_0 = 0.9927a$. Not surprisingly, these two solutions gave almost the same results in a wide range as demonstrated in Figure 6, which validates the accuracy of the present solution for Case 1.

4.2. Comparison with Solution for Circular Cavity. Providing that the initial and the final shapes of the inner cavity are both circular ($a_0 = b_0 = R_0$) and the far-field stress conditions are hydrostatic (i.e., axisymmetric stress and geometry conditions), the presented displacement-controlled solutions can give the same results as the conventional stress-controlled solution (e.g., equation (36) to (38) from Yu [1]), and solutions for Cases 1 and 2 become identical in this special case. As demonstrated in Figure 7, results calculated with these three solutions agree well in this simplified condition.

$$\sigma_r = -P_\infty - (p_{in} - P_\infty)\frac{R_0^2}{r^2}, \tag{36}$$

$$\sigma_\theta = -P_\infty + (p_{in} - P_\infty)\frac{R_0^2}{r^2}, \tag{37}$$

$$u_r = \frac{-(p_{in} - P_\infty)}{2G}\frac{R_0^2}{r}r. \tag{38}$$

4.3. Comparison of Stress and Displacement Fields. Except at the vertices, the normal direction of points on an ellipse does not coincide with the normal direction, and this difference would be intensified with increases of a/b. Therefore, the formed stress field around the ellipse calculated with the previously developed two displacement-controlled solutions would be different. Taking $a/b = 5/3$ as an example, with the same soil properties and cavity positions (initial and final), results calculated with these two solutions are presented in Figures 8 and 9, respectively ($G = 20$ MPa, Poisson's ratio $\nu = 0.4$).

The directions of displacements at the inner ellipse for Case 1 are more paralleling to the major axis direction of

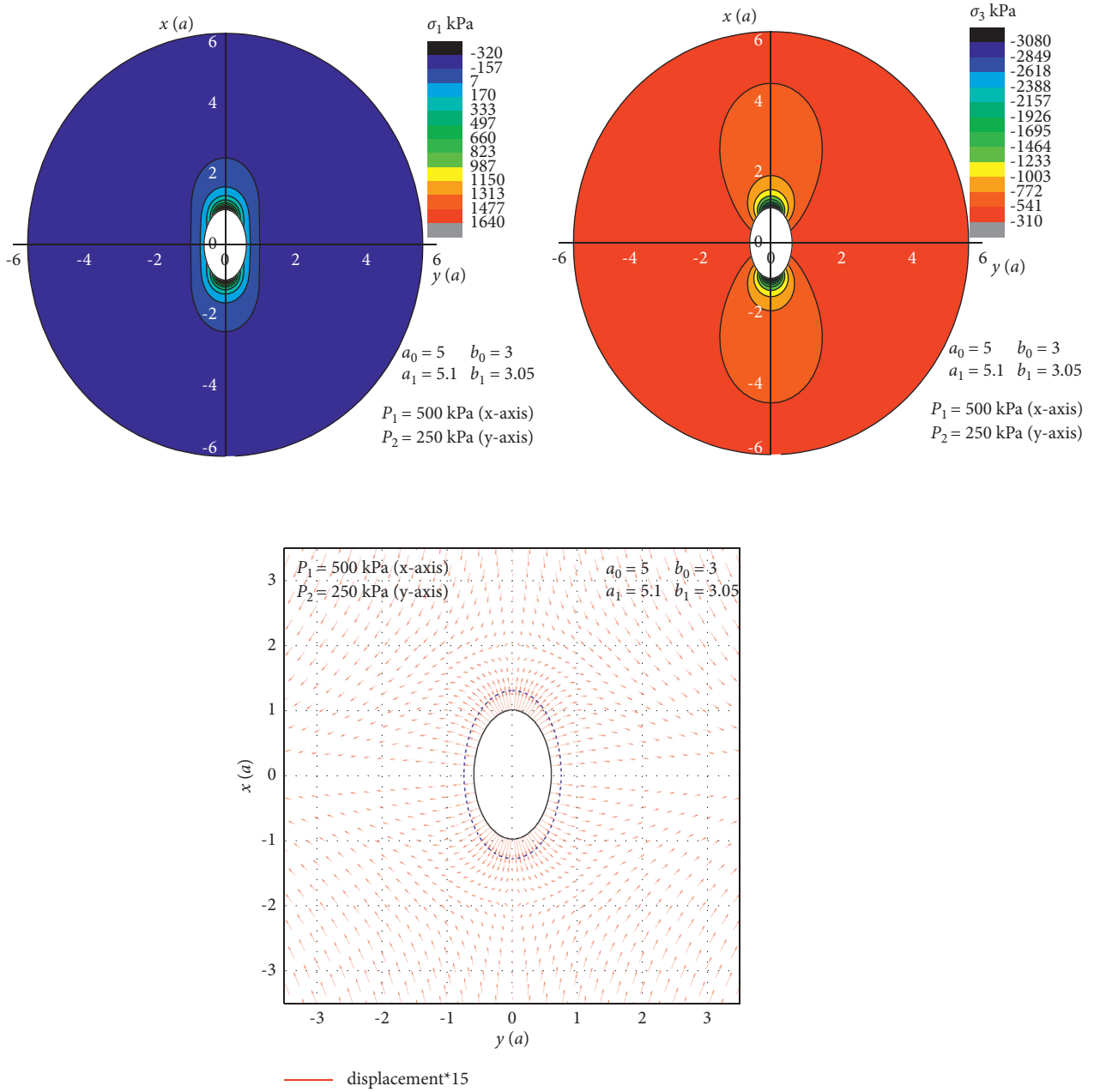

Figure 8: Stress and displacement fields around an ellipse (Case 1).

the ellipse than those of Case 2. This difference leads to significant variations of the surrounding stress fields although the initial and final positions of the ellipse were set as the same in these two solutions. Specifically, with given displacements normal to the initial ellipse, tensile zones are concentrated around vertices of the major axis. The plate around the ellipse seems to be stretched in the direction paralleling the minor axis of the ellipse (Figure 8). On the contrary, tensile zones emerged from vertices of the minor axis when the boundary points were set to move along radial directions (Figure 9). The plate seems to be stretched in the direction paralleling the major axis of the ellipse. In addition, the magnitude and concentration degree of the stresses caused by different types of displacement boundary conditions are distinctly different as well.

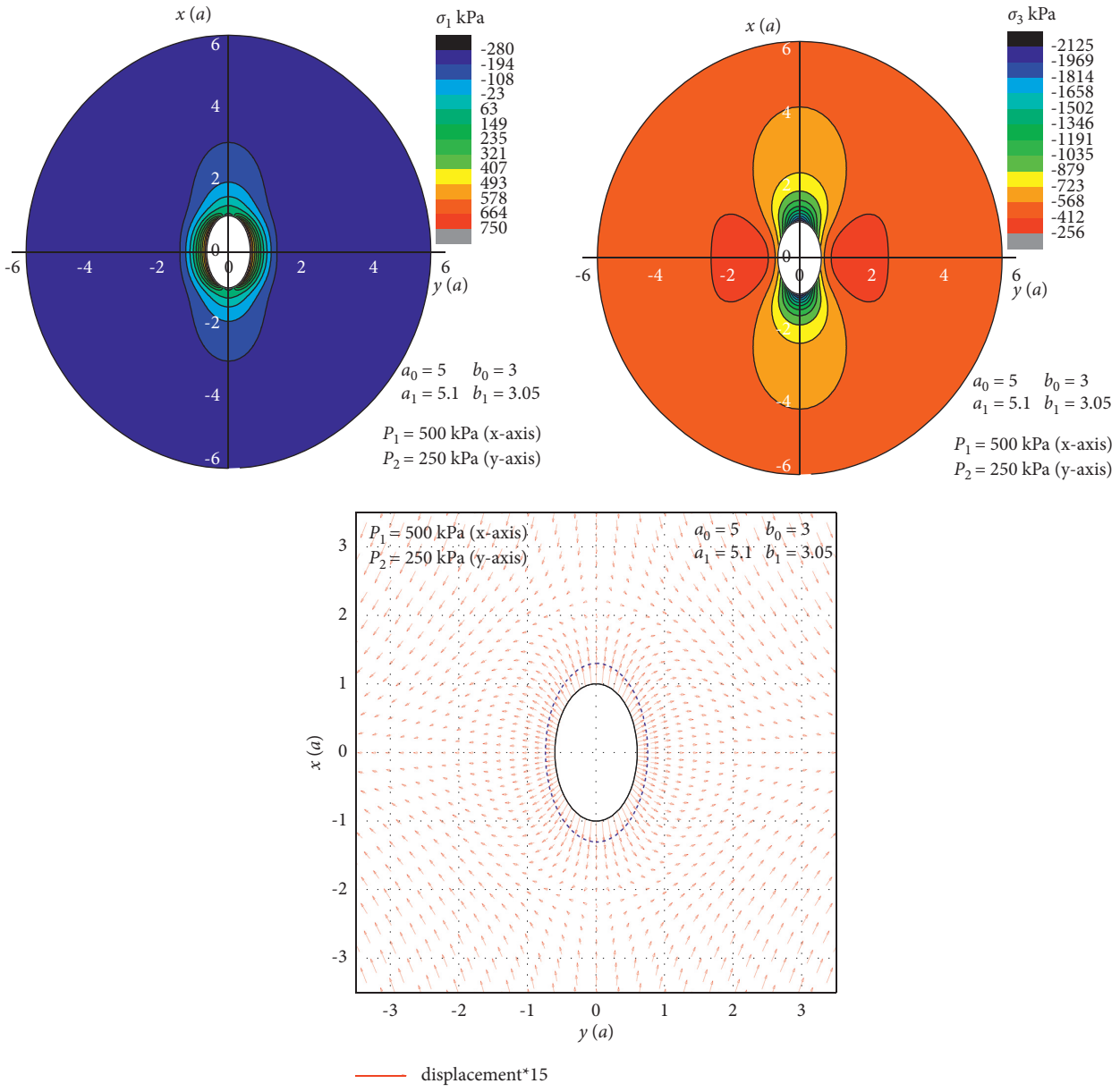

Figure 9: Stress and displacement fields around an ellipse (Case 2).

5. Conclusions

Analytical solutions for the calculation of stresses and displacements caused by specified deformation of an elliptical cavity in an infinite plane with biaxial far-field stresses are developed using the complex variable theory for plane elasticity in this paper. A general method dealing with displacement boundary conditions is presented by means of the combined use of the conformal mapping technique and Fourier series in complex form, and the Kolosov-Muskhelishvili complex potentials were obtained using Cauchy's integral formula. Two typical displacement-controlled boundary conditions (i.e., normal to the inner cavity and outwards from the centre of the inner cavity) are analysed with the proposed method, and it is found that stresses and displacements induced by inner cavity deformation depend both on the magnitude and the direction of soil particle movement. The new solutions may be useful in many engineering problems such as analysis of stress concentration/strain localisation around an elliptical hole/opening in linear elastic materials and interaction between soils and man-made penetrometers (e.g., flat dilatometer) and living organisms in nature (e.g., plant roots and earthworms).

Data Availability

Some or all data, models, or code generated or used during the study are available from the corresponding author by request.

Conflicts of Interest

The authors declare that they have no conflicts of interest.

Acknowledgments

This work was supported by the National Natural Science Foundation of China (52108374), the "Taishan" Scholar Program of Shandong Province, China (tsqn201909016), and the Shandong Provincial Natural Science Foundation (ZR202102250562).

References

[1] H. S. Yu, *Cavity Expansion Methods in Geomechanics*, Kluwer Academic Publishers, The Netherlands, 2000.

[2] G. N. Savin, *Stress distribution around holes*, national aeronautics and space administration, Washington, D.C, USA, 1970.

[3] N. I. Muskhelishvili, *Some Basic Problems of the Mathematical Theory of Elasticity*, P. Noordhoff, Groningen, Netherlands, 4th Ed. edition, 1963.

[4] A. P. S. Selvadurai, *Partial differential equations in mechanics 2*, springer science & business media, Berlin, Germany, 2000.

[5] A. E. H. Love, *A Treatise on the Mathematical Theory of Elasticity*, Cambridge University Press, , London, UK, 4th Ed. edition, 1927.

[6] A. S. Saada, *Elasticity: theory and applications*, Pergamon Press, Inc, Oxford, UK, 1974.

[7] S. P. Timoshenko and J. N. Goodier, *Theory of Elasticity*, McGraw-Hill, Inc<, , London, UK, 3rd Ed. edition, 1970.

[8] C. E. Inglis, "Stresses in a plate due to the presence of cracks and sharp corners," *Spie Milestone series MS*, vol. 137, pp. 3–17, 1913.

[9] A. A. Griffith, "The phenomena of rupture and flow in solids. Philosophical transactions of the royal society of london," *Series A, containing papers of a mathematical or physical character*, vol. 221, pp. 163–198, 1921.

[10] A. C. Stevenson, "Complex potentials in two-dimensional elasticity. Proceedings of the royal society of london," *Series A. Mathematical and Physical Sciences*, vol. 184, no. 997, pp. 129–179, 1945.

[11] O. E. Strack, *Analytic Solutions of Elastic Tunneling Problems*, Delft University of Technology, Delft, Netherlands, 2002.

[12] C. Sagaseta, "Analysis of undrained soil deformation due to ground loss," *Géotechnique*, vol. 37, no. 3, pp. 301–320, 1987.

[13] A. Verruijt, "A complex variable solution for a deforming circular tunnel in an elastic half-plane," *International Journal for Numerical and Analytical Methods in Geomechanics*, vol. 21, no. 2, pp. 77–89, 1997.

[14] D. Maugis, "Stresses and displacements around cracks and elliptical cavities: exact solutions," *Engineering Fracture Mechanics*, vol. 43, no. 2, pp. 217–255, 1992.

[15] H.-C. Wu and K.-J. Chang, "Angled elliptic notch problem in compression and tension," *Journal of Applied Mechanics*, vol. 45, no. 2, pp. 258–262, 1978.

[16] E. Atroshchenko, *Stress Intensity Factors for Elliptical and Semi-elliptical Cracks Subjected to an Arbitrary Mode I Loading*, University of Waterloo, Ontario, Canada, 2010.

[17] H. Zhou, G. Q. Kong, P. Li, and H. Liu, "Flat cavity expansion: theoretical model and application to the interpretation of the flat dilatometer test," *Journal of Engineering Mechanics*, vol. 142, no. 1, Article ID 04015058, 2015.

[18] E. C. Aifantis, "Higher Order Gradients and Size Effects," in *Size-scale Effects in the Failure Mechanisms of Materials and Structures*, A. Carpinteri, Ed., pp. 231–242, E & FN Spon, London, UK, 1996.

[19] B. H. Brady, *Rock mechanics: for underground mining*, springer science & business media, Springer, Germany, 2004.

[20] E. Detournay and C. M. John, "Design charts for a deep circular tunnel under non-uniform loading," *Rock Mechanics and Rock Engineering*, vol. 21, no. 2, pp. 119–137, 1988.

[21] P. Foray, L. Balachowski, and G. Rault, "Scale effects in shaft friction due to the localization of deformations," in *Proceedings of the International Conference Centrifuge*, Tokyo, Japan, September 1998.

[22] J. P. Turner and F. H. Kulhawy, "Physical modeling of drilled shaft side resistance in sand," *Geotechnical Testing Journal*, vol. 17, no. 3, pp. 282–290, 1994.

[23] E. Wernick, "Skin friction of cylindrical anchors in non-cohesive soils," in *Proceedings of the symposium on soil reinforcing and stabilising techniques*, Sydney, Australia, Octobar, 1978.

[24] A. Patel and C. K. Desai, "Stress concentration around an elliptical hole in a large rectangular plate subjected to linearly varying in-plane loading on two opposite edges," *Theoretical and Applied Fracture Mechanics*, vol. 106, Article ID 102432, 2020.

[25] X. L. Gao, "A general solution of an infinite elastic plate with an elliptic hole under biaxial loading," *International Journal of Pressure Vessels and Piping*, vol. 67, no. 1, pp. 95–104, 1996.

[26] H. Zhou, G. Kong, and H. Liu, "Pressure-controlled elliptical cavity expansion under anisotropic initial stress: elastic solution and its application," *Science China Technological Sciences*, vol. 59, no. 7, pp. 1100–1119, 2016.

[27] P. Z. Zhuang, *Cavity Expansion Analysis with Applications to Cone Penetration Test and Root-Soil Interaction*, University of Nottingham, Nottingham, UK, 2017.

[28] H. Zhou, H. Liu, and Z. Wang, "A semi-analytical solution for displacement-controlled elliptical cavity expansion in undrained MCC soil," *International Journal for Numerical and Analytical Methods in Geomechanics*, vol. 46, no. 2, pp. 339–373, 2021.

[29] K. A. Daltorio and A. Boxerbaum, "Efficient worm-like locomotion: slip and control of soft-bodied peristaltic robots," *Bioinspiration & Biomimetics*, vol. 8, no. 3, Article ID 035003, 2013.

[30] S. Marchetti, "The flat dilatometer: design applications," in *Proceedings of the Third International Geotechnical Engineering Conference*, Cairo University, Cario, Egypt, January. 1997.

[31] J. D. Lawrence, *A Catalog of Special Plane Curves*, Mineola, Dover, UK, 1972.

[32] D. J. Unger, "Large plastic deformations accompanying the growth of an elliptical hole in a thin plate," *Journal of Elasticity*, vol. 99, no. 2, pp. 117–130, 2010.

[33] D. J. Unger, "Perfectly plastic caustics for the opening mode of fracture," *Theoretical and Applied Fracture Mechanics*, vol. 44, no. 1, pp. 82–94, 2005.

[34] A. H. England, *Complex Variable Methods in Elasticity*DoverPublications, Inc, New York, USA, 2003.

[35] I. S. Sokolnikoff, *Mathematical theory of elasticity*, McGraw-Hill, New York, USA, 1956.